

# Supporting Information of

## Control of the polarization of ferroelectric capacitors by the concurrent action of light and adsorbates

*Fanmao Liu,<sup>†</sup> Ignasi Fina,<sup>\*,†</sup> Guillaume Sauthier,<sup>‡</sup> Florencio Sánchez,<sup>†</sup> Andrew M. Rappe,<sup>§</sup> Josep  
Fontcuberta<sup>†</sup>*

<sup>†</sup>Institut de Ciència de Materials de Barcelona (ICMAB-CSIC), Campus UAB, Bellaterra 08193,  
Catalonia, Spain

<sup>‡</sup>Catalan Institute of Nanoscience and Nanotechnology (ICN2), CSIC and The Barcelona Institute of  
Science and Technology, Campus UAB, Bellaterra 08193, Catalonia, Spain

<sup>§</sup>Department of Chemistry, University of Pennsylvania, Philadelphia, Pennsylvania 19104-6323,  
United States

\*ignasifinamartinez@gmail.com

## Further Methods Details

*BTO/LSMO bilayers were grown in a single process by pulsed laser deposition on (001) SrTiO<sub>3</sub> and (110) DyScO<sub>3</sub> substrates (5 × 5 × 0.5 mm) using a KrF excimer laser ( $\lambda = 248$  nm) and stoichiometric targets. The LSMO film was grown at 725 °C under an oxygen pressure of 0.2 mbar and a laser repetition rate of 2 Hz. The growth of BTO was performed at 700 °C and with an oxygen pressure of 0.02 mbar and 2 Hz of laser frequency. The growth rate of per laser pulse is 0.12 Å p<sup>-1</sup> and 0.35 Å p<sup>-1</sup> for LSMO and BTO, respectively. After growing the samples, top 20 nm platinum electrodes of 60 × 60 μm<sup>2</sup> and with 15 μm distance separating each were deposited ex-situ on the BTO surface by sputtering. Detailed structural characterization of the whole set of samples showing no-correlation between structural parameters and  $\Delta P_r$  is summarized in Supporting Information Figure S3-4.*

*The ferroelectric measurements were conducted, at room temperature, in top-top configuration, where one top electrode was biased and the other was grounded.<sup>1-2</sup> The two electrodes used in t-t are always adjacent. Ferroelectricity was characterized by applying triangular  $V-t$  pulses at a fixed frequency of 1 kHz, and measuring the dynamic  $I-V$  hysteresis loops, using a TFAalyzer2000 (aixACCT Systems GmbH) to determine the switchable polarization  $P$ . The electric field is evaluated as  $E = V / (2\delta)$  for the t-t configurations ( $\delta$  is the ferroelectric film thickness).*

*$P-E$  loops measured under illumination were collected by shining the electrodes with a laser of wavelength 405 nm feed by a CPX400SA DC power source (AimTTi Co.). The used photons (3.06 eV)*

are of sub-bandgap energy (3.3 eV for BTO<sup>3</sup>). The spot diameter is of 200  $\mu\text{m}$ , which largely covers two electrodes, allowing a homogeneous illumination with a power of 10  $\text{W}\cdot\text{cm}^{-2}$ .

*XPS measurements* were performed with a Phoibos 150 analyzer (SPECS GmbH) in ultra-high vacuum conditions (base pressure  $4\times 10^{-10}$  mbar) with a monochromatic aluminum  $\text{K}_\alpha$  x-ray source (1486.74 eV). The energy resolution as measured by the FWHM of the Ag 3d5/2 peak for a sputtered silver foil was 0.62 eV. Samples were fixed on the sample holder by metallic screws that were grounded. The samples have been exposed to air between when transferred from the growth chamber to the XPS chamber. Therefore, a clear C contamination was found in all spectra. (see Supporting Information Figure S13). The take-off angle was always 90°. The data were analysed by the software CasaXPS<sup>4</sup>. The binding energy was corrected by using the C-1s line at 284.6 eV as the reference. Curve fitting was performed using Gaussian/Lorentzian (70/30) ratio for all peaks. Full width at half maximum (FWHM) was constrained at  $1.5\pm 0.2$  eV and peak position at  $\pm 0.1$  eV fluctuations. Shirley algorithm was used to subtract the background before data fitting. The percentage of each specie (I<sub>o</sub>, I, II, III) is defined as:  $A(j) (\%) = A(j) / A(\text{Tot})$  ( $j = \text{I}_o, \text{I}, \text{II}, \text{III}$ ), where  $A(j)$  and  $A(\text{Tot})$  indicate the area of  $j$  component and the total area of whole O1s spectrum above the background.

*Steam treatment* experiment was using a YiDu PTC heater at ambient pressure and room temperature surroundings. The deionized water kept boiling in the glass bottle during the experiment. The thin film sample was hanging upon the bottle with the sample plane parallel to the water flux (see Supporting Information Figure S14).

*Ferroelectric loops simulations* were done using the  $E_f = E - \frac{d}{t} \frac{P(E_f)}{\epsilon_0 \epsilon_d}$  equation<sup>5</sup> for a ferroelectric

layer of thickness  $t$  containing a dielectric interface layer (non-ferroelectric) of thickness  $d$  for the calculation of the effective applied field to the ferroelectric ( $E_f$ ) as a function of the external applied field ( $E$ ), where  $\epsilon_0$  corresponds to the vacuum dielectric permittivity, and  $P(E_f)$  the polarization of the ferroelectric layer as a function of  $E_f$ . For our simulation we used

$P(E_f) \cong P_{f,s} \tanh\left(\frac{E_f - E_c}{\delta}\right) + \epsilon_0 \epsilon_f E_f$  that accounts for the polarization of the ferroelectric with  $P_{f,s}$

being the saturation polarization of the ferroelectric ( $26 \mu\text{C}/\text{cm}^2$ ),  $E_c$  the coercive field (350 kV/cm), and  $\delta$  the amplitude of the coercive field (100 kV/cm), and  $\epsilon_f$  is the dielectric permittivity (300). Further details are in Supporting Information Figure S10.

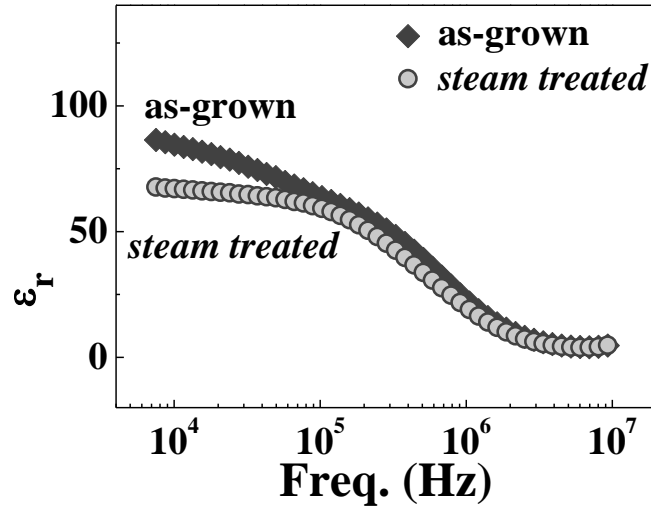


**Figure S1.** Dependence of the relative dielectric permittivity ( $\epsilon_r$ ) of the film in dark on frequency in Pt electrodes deposited before and after the steam treatment. From the frequency-dependent dielectric permittivity measurement, further evidence of the important role of adsorbates is obtained. It is well known that the low-frequency capacitance in metal/dielectric/metal structures can be severely affected by parasitic interface capacitance and thus it can be used as a fingerprint of their presence.<sup>6-11</sup> In the Figure, we show the permittivity of the Pt/BTO/LSMO film with Pt contacts deposited either on the fresh BTO surface (solid symbols) or after *steam treatment* (empty symbols). It is clear that at low frequency, the capacitance of the *steam treated* structure is smaller than in the pristine sample, which as analyzed in detail in previous literature<sup>6-11</sup>, indicates than in the former there is a series interface capacitance. The frequency dependence of dielectric permittivity observed in the whole frequency range is commonly attributed to electronic conduction.<sup>7</sup>

The dielectric permittivity was extracted from impedance measurements at room temperature using a LF4182 impedance analyzer (Agilent Co.). The extracted capacitance was that corresponding to a parallel resistance-capacitor circuit, corresponding to a dielectric layer with sizable conductivity, as it is applicable for our film in parallel with the capacitor. Dielectric permittivity was obtained from out-of-phase component of the impedance by using  $C = \epsilon A / 2t$ , where  $C$  is the measured capacitance,  $A$  is the area of the electrode and  $t$  is the thickness of the film. The frequency range available in our set up ranges from 5Hz to 13 MHz; however at low frequencies ( $< 8$  kHz) measurements were not possible because the exceedingly large overall impedance of the measured device.

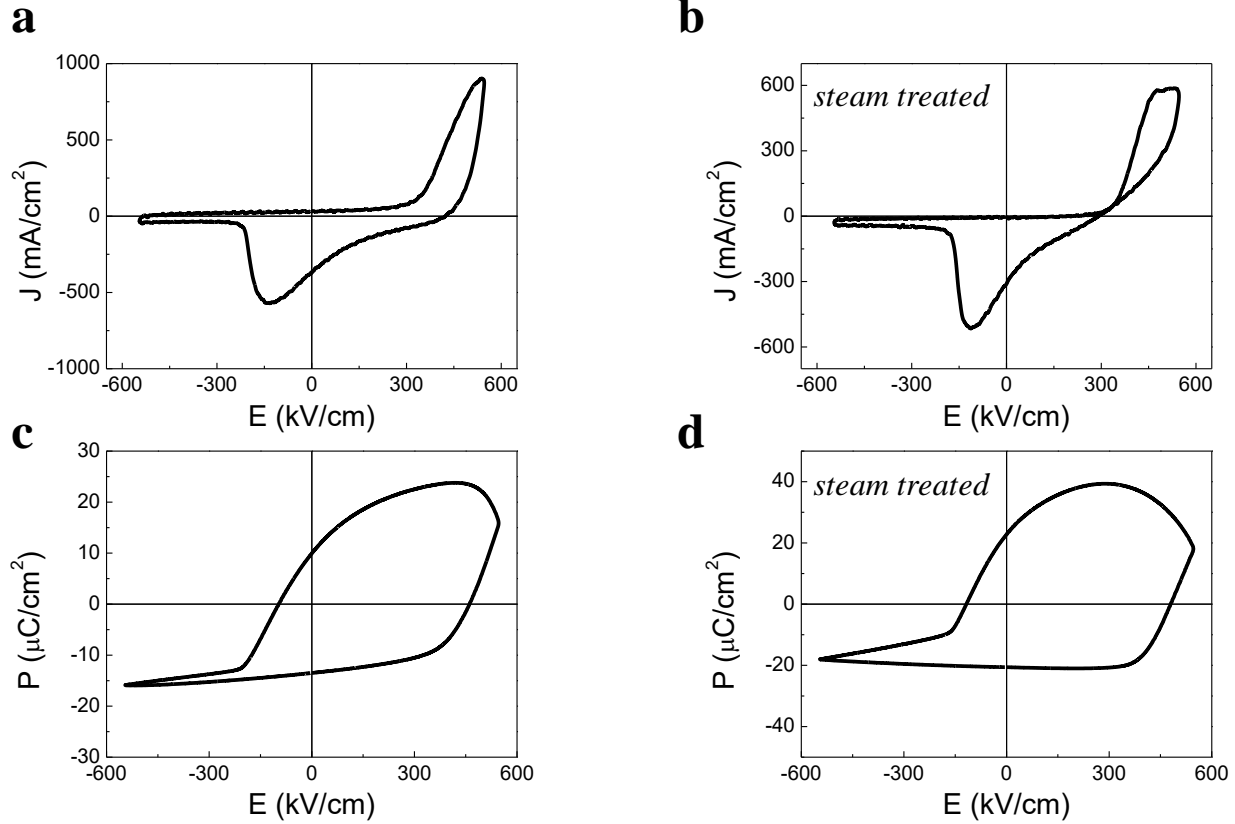


**Figure S2.** (a,c) J-E loops and (c,d) loops of 109.5 nm BTO/LSMO//DSO sample, in dark, obtained (a,c) before and (b,d) after steam treatment. (b,d) P-E loops in dark and under illumination with top electrodes deposited after 10 h steam treatment, for 109.5 nm BTO/LSMO//DSO and 50 nm BTO/LSMO/STO samples, respectively. It can be noticed a small shift towards positive electric field.

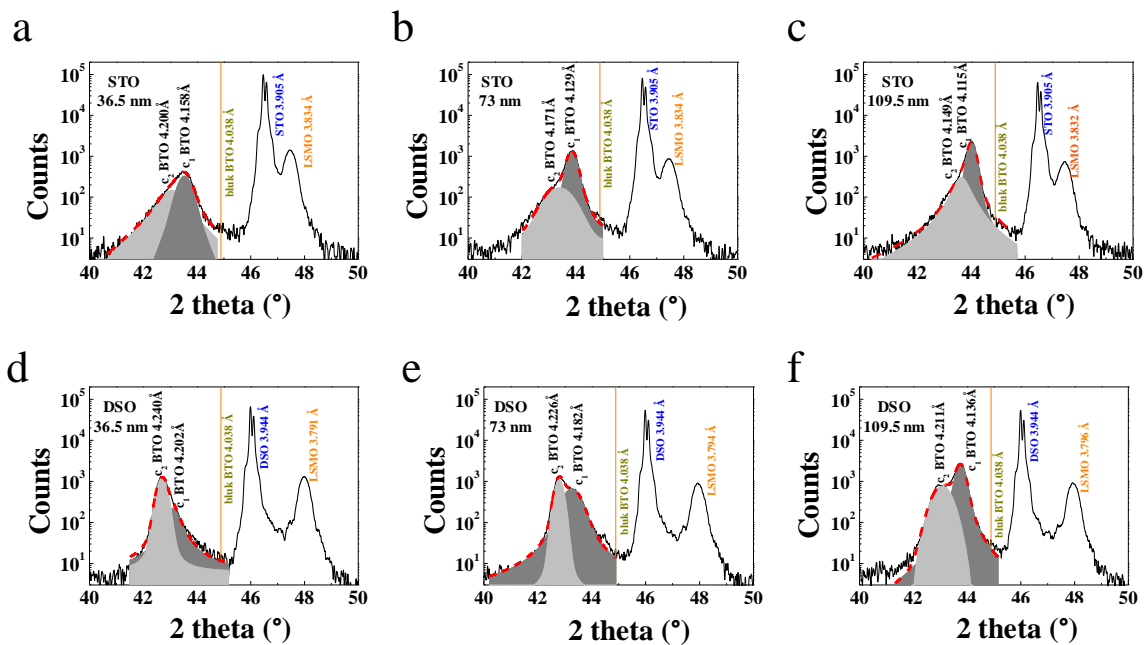


**Figure S3.** XRD 2-theta scan spectrum of (a,b,c) 36.5, 73 and 109.5 nm samples grown on LSMO//STO substrate (d,e,f) 36.5, 73 and 109.5 nm samples grown on /LSMO//DSO substrate, respectively. The dark and light grey region under the peak of BTO correspond to the fitting by two Gaussian curves of the data.

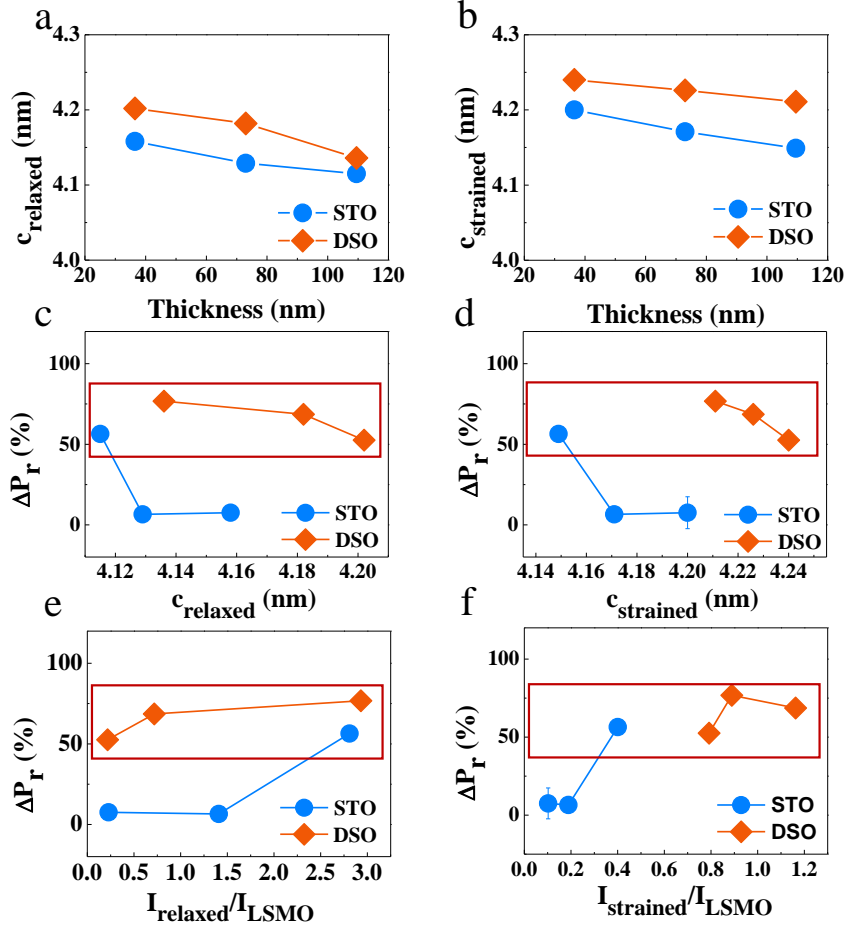


**Figure S4.** Out of plane parameters for both phases: (a)  $c_{\text{relaxed}}$  and (b)  $c_{\text{strained}}$  extracted by Gaussian fitting from the XRD 2-theta scan spectrum of Figure S1. Dependence of  $\Delta P_r$  on relaxed and strained phase: (c,d)  $\Delta P_r$  versus  $c_{\text{relaxed}}$  and  $c_{\text{strained}}$  values, respectively. (e,f)  $\Delta P_r$  versus the intensity of the relaxed ( $I_{\text{relaxed}}$ ) and strained ( $I_{\text{strained}}$ ) peaks, respectively, extracted from the Gaussian fitting, normalized to the LSMO peak intensity ( $I_{\text{LSMO}}$ ). Note that  $c_{\text{relaxed}}$  and  $c_{\text{strained}}$  values are larger than  $\text{BaTiO}_3$  bulk value ( $c = 4.038 \text{ \AA}$ ), which we attribute not only to the larger tetragonality but also to oxygen vacancies as revealed by XRD reciprocal lattice maps of equivalent samples reported in previous works.<sup>12</sup>

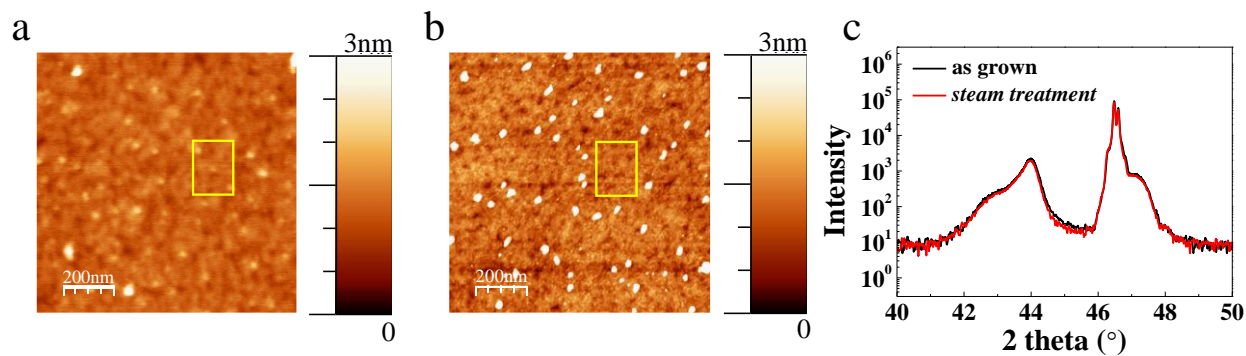


**Figure S5.** AFM surface topography image collected for the 109.5 nm BTO film grown on LSMO//STO substrate, (a) before and (b) after the *steam treatment*, corresponding to the sample and results shown in Figure 6 of the main text. The RMS values extracted from the area enclosed by the yellow rectangle in (a) and (b) are 0.22 and 0.25 nm, respectively (c) XRD 2theta scan spectra, before and after *steam treatment*.

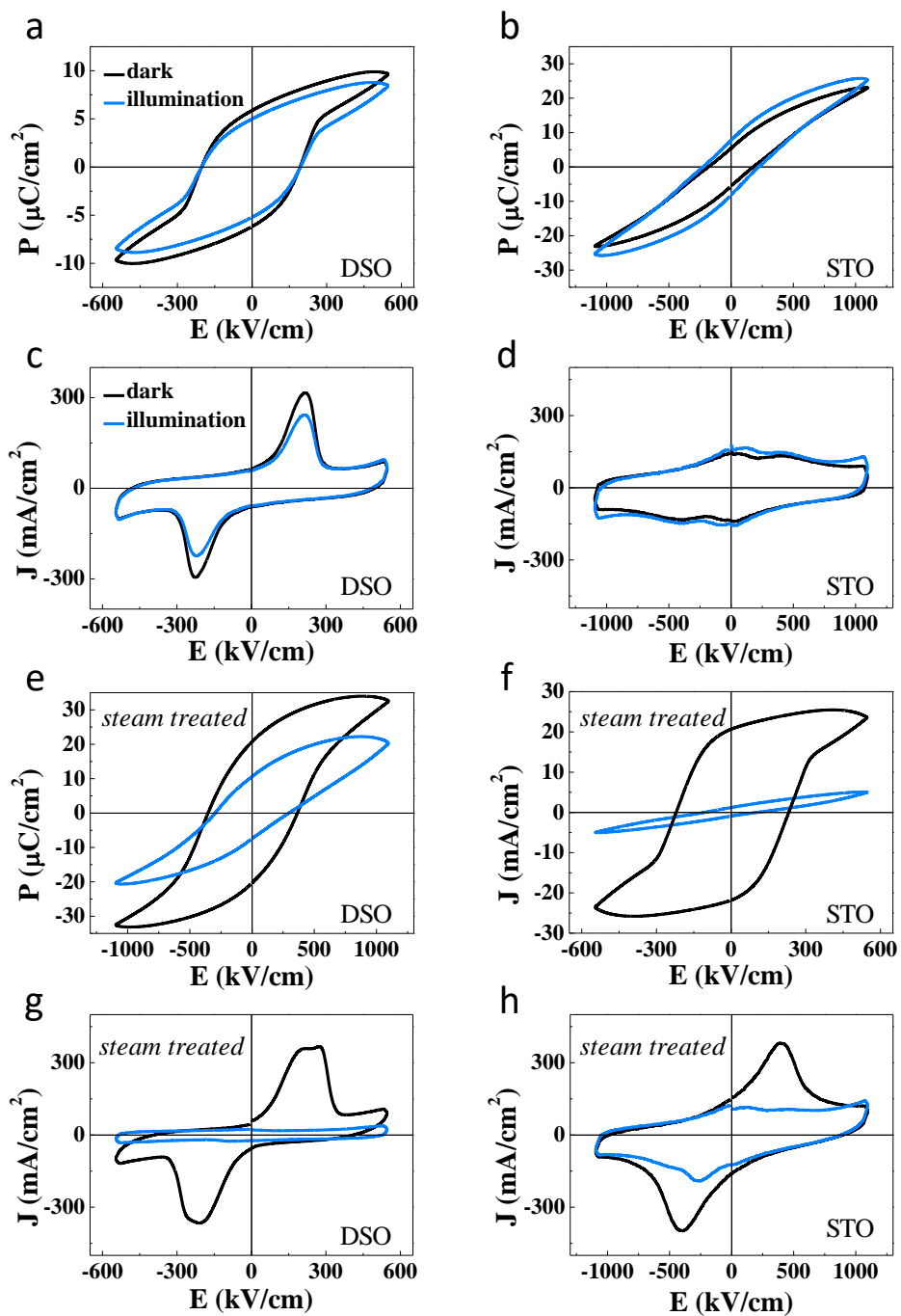


**Figure S6.** (a,b) P-E and J-E (c,d) loops of 109.5 nm BTO/LSMO//DSO and 50 nm BTO/LSMO//STO samples, in dark and under illumination, obtained before steam treatment. (e,f) P-E and (g,h) loops in

dark and under illumination with top electrodes deposited after 10 h *steam treatment*, for 109.5 nm BTO/LSMO//DSO and 50 nm BTO/LSMO/STO samples, respectively. All the loops were recorded in *t-t* configuration. It can be inferred from J-E loops of steam treated samples (g,h) that only the reduction of the ferroelectric switching current, which corresponds to the positive and negative current peaks apparent at  $\pm 300$  and  $\pm 500$  kV/cm, respectively, dominates to the reduction of the integrated polarization of panels (b,d). Thus, the effect of conductivity changes under illumination can be disregarded as a dominant effect in the observed reduction of  $P_r$ . Small conductivity changes under illumination compared to the ferroelectric switching polarization decrease have been observed in samples of different thicknesses which P-E loops are included in Figure S9.

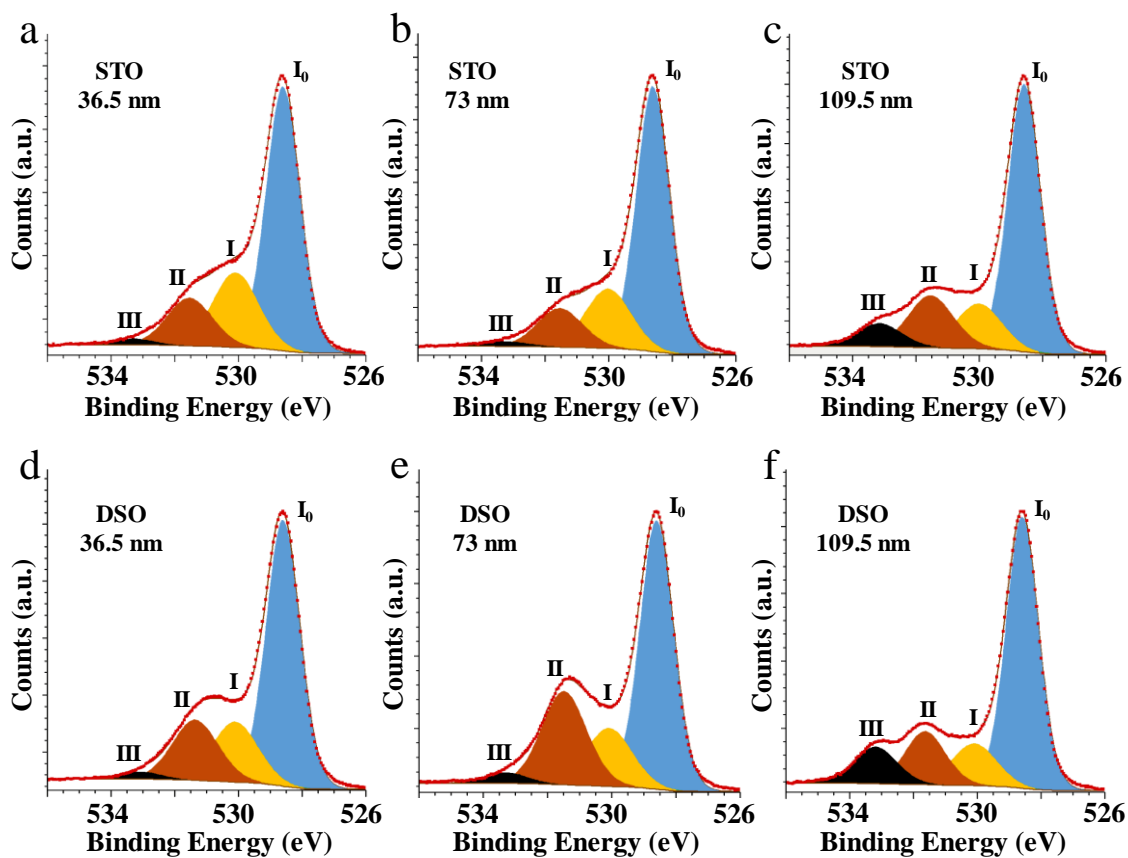


**Figure S7.** XPS spectra of O 1s core level (red dots). (a,b,c) 36.5, 73 and 109.5 nm BTO films on LSMO//STO, respectively. (d,e,f) 36.5, 73 and 109.5 nm BTO films on LSMO//DSO, respectively. Data fitting (see Methods) was performed by decomposing the spectra by 4 different contributions (labelled I<sub>0</sub>, I, II, and III) as indicated. The sum of the four components of the best fit is indicated by a continuous (brown) line.

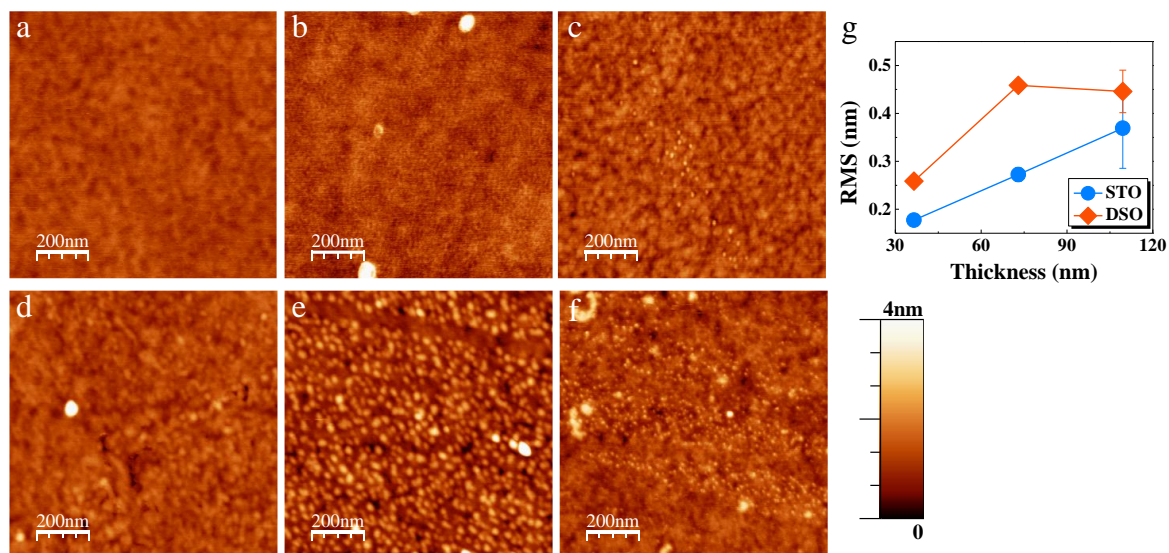


**Figure S8.** (a-f) AFM topography images ( $2 \mu\text{m} \times 2 \mu\text{m}$ ) of BTO films of thicknesses 36.5nm, 73nm, 109.5nm grown on STO (a,b,c) and DSO (d,e,f) respectively. White dots seem to be more present in thicker samples denote the increasing presence of adsorbates as thickness increases. (g) Surface roughness (RMS) vs film thickness. Therefore, we found that the measured roughness of all films increases very modestly from 0.2 to 0.5 nm for BTO/LSMO//STO films and a similar trend is found for BTO/LSMO//DSO films, although with marginally larger RMS values (0.3 – 0.7 nm). Therefore, although there is some enhancement of specific surface with thickness, which is even more pronounced in BTO films on DSO substrates, the observation of an opposite trend for the evolution of I ( $\text{BaCO}_3$ ) and II+III ( $\text{H}_2\text{O}/\text{OH}^-$ ) species with thickness denies that changes of specific surface are at the root of this observation.

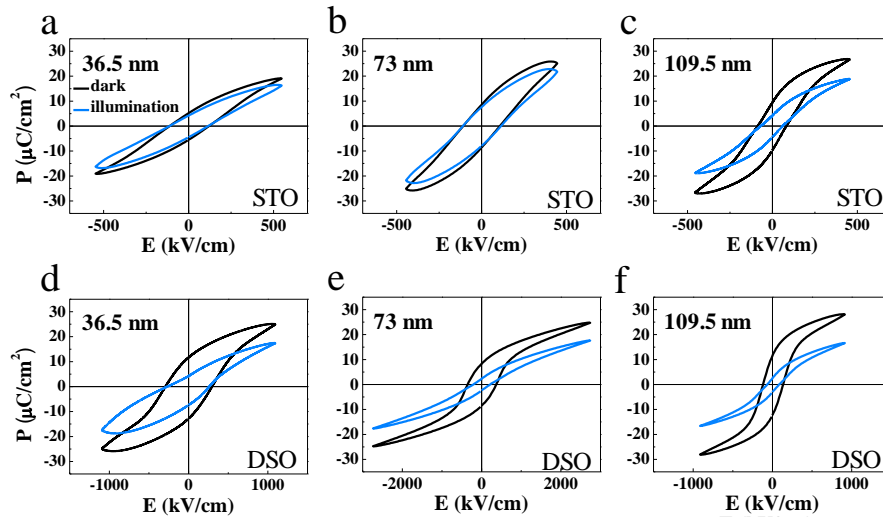


**Figure S9.** Polarization loops recorded in dark and under illumination (black and blue lines, respectively) of BTO films different thicknesses (36.5 nm, 73 nm, 109.5 nm) grown on different substrates (STO and DSO). (a-c) loops recorded on BTO/LSMO//STO; (d-f) loops recorded on BTO/LSMO//DSO. Note that, whereas the  $P_r$  values among the samples are very similar (except for the case of the 36.5nm sample grown on STO), the corresponding  $\Delta P_r$  values are not, thus suggesting that the magnitude of the dark  $P_r$  does not play a fundamental role on the observed photoresponse.

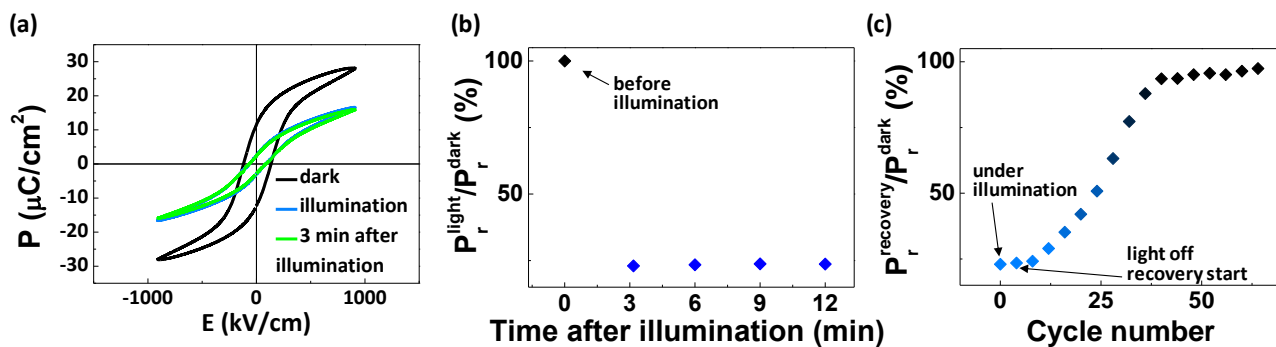


**Figure S10.** (a) P-E loops collected in dark, under illumination and after waiting 3 min in dark after illumination. (b)  $P_r$  relative to its initial value in dark versus delay time in dark after illumination. The  $P_r$  value measured in initial dark conditions is also indicated. (c)  $P_r$  relative to its initial value in dark versus electric field (400 kV/cm) bipolar cycling number. All data have been collected for the 109.5 nm sample grown on DSO.

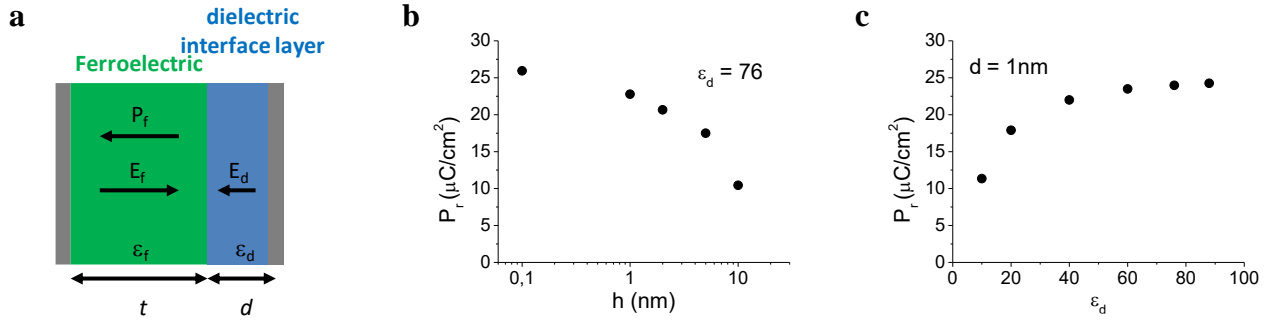


**Figure S11.** (a) Model for a ferroelectric (with dielectric constant  $\epsilon_f$  and thickness  $t$ ) plus a dielectric (no-ferroelectric) interface layer (with dielectric constant  $\epsilon_d$  and thickness  $d$ ) where grey areas represent metallic electrodes. Based on this model the relation between the external applied field ( $E$ ) and the effective applied field to the ferroelectric ( $E_f$ ) can be extracted as in ref. 5, and reads as follows:

$$E_f = E - \frac{d}{h} \frac{P(E_f)}{\epsilon_0 \epsilon_d},$$

where  $\epsilon_0$  corresponds to the vacuum dielectric permittivity. To simulate the

main manuscript ferroelectric loops we have used the following equation

$$P(E_f) \cong P_{f,s} \tanh\left(\frac{E_f - E_c}{\delta}\right) + \epsilon_0 \epsilon_f E_f,$$

where the first part accounts for the ferroelectric hysteretic part

with  $P_{f,s}$  being the saturation polarization of the ferroelectric ( $26 \mu\text{C}/\text{cm}^2$ ),  $E_c$  the coercive field (350 kV/cm), and  $\delta$  the amplitude of the coercive field (100 kV/cm), and the second part accounts for the

linear dielectric response of the ferroelectric, where  $\epsilon_f$  is the dielectric permittivity (300). In the here

shown and main manuscript simulations, the value for the ferroelectric layer thickness has been taken

as 109.5nm. (b) Results of the  $P_r$  value of several simulated loops fixing the dielectric interface layer

permittivity to 76 (similar to the water permittivity at 30°C<sup>13</sup>) and varying the dielectric interface layer thickness from 0.1 to 10 nm. (c) Results of the  $P_r$  value of several simulated loops fixing the dielectric interface layer thickness to 1 nm and varying the dielectric interface layer permittivity from 10 to 90. In (b,c) it can be observed that the  $P_r$  increases while increasing the dielectric interface layer thickness or decreasing the dielectric interface layer permittivity, as expected. We observed that only for thickness values around 10 nm the reduction of  $P_r$  is as large as 60%, and for 1 nm film a reduction of 60% is achieved with dielectric interface layer permittivity of 10.

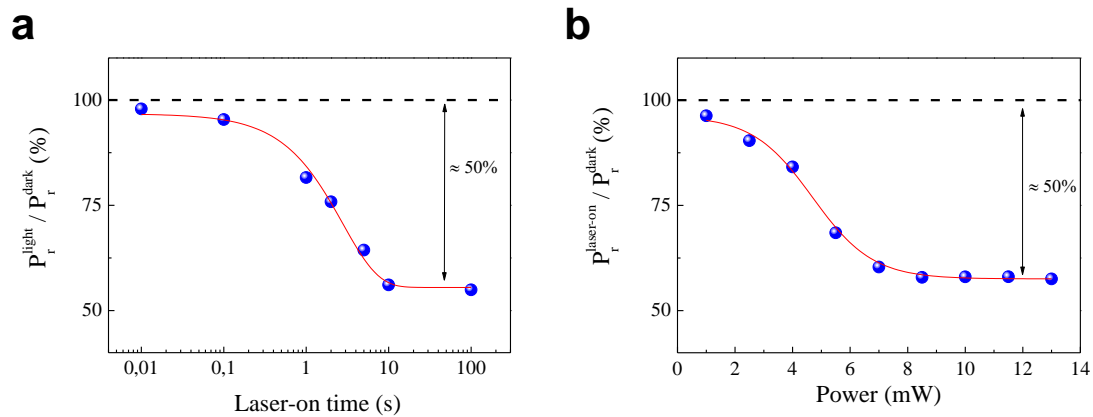


**Figure S12.** Normalized variation of  $P_r$  for different (a) illumination times at 10mW, and (b) power after 10s respect to its initial value in dark.

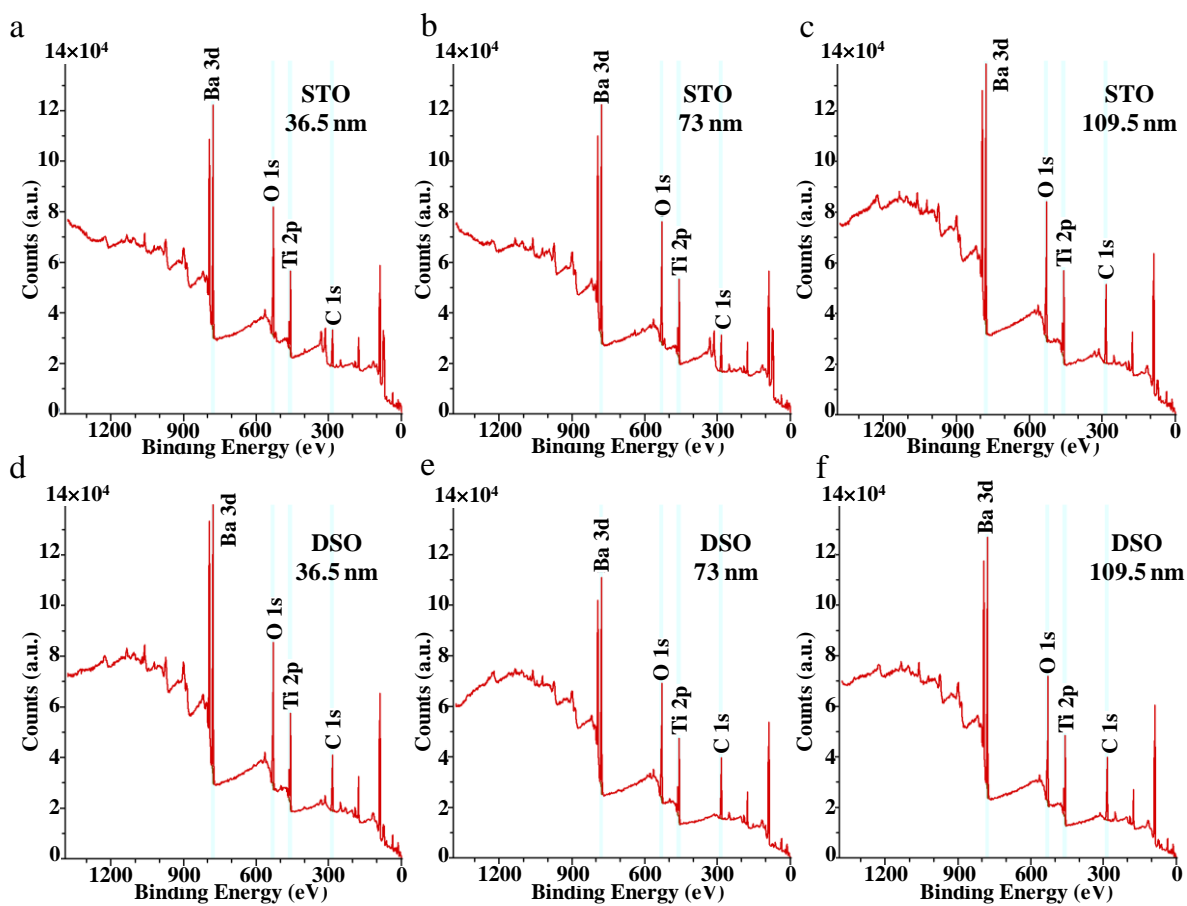


**Figure S13.** Survey XPS spectra of BTO films different thicknesses (36.5 nm, 73 nm, 109.5 nm) grown on STO (a,b,c) and DSO (d,e,f) showing the presence C peaks.

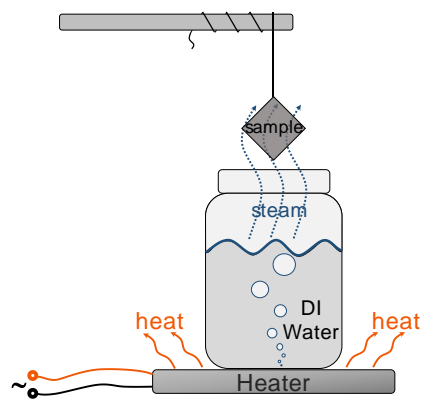


**Figure S14.** Schematic diagram of the steam exposure experiment.

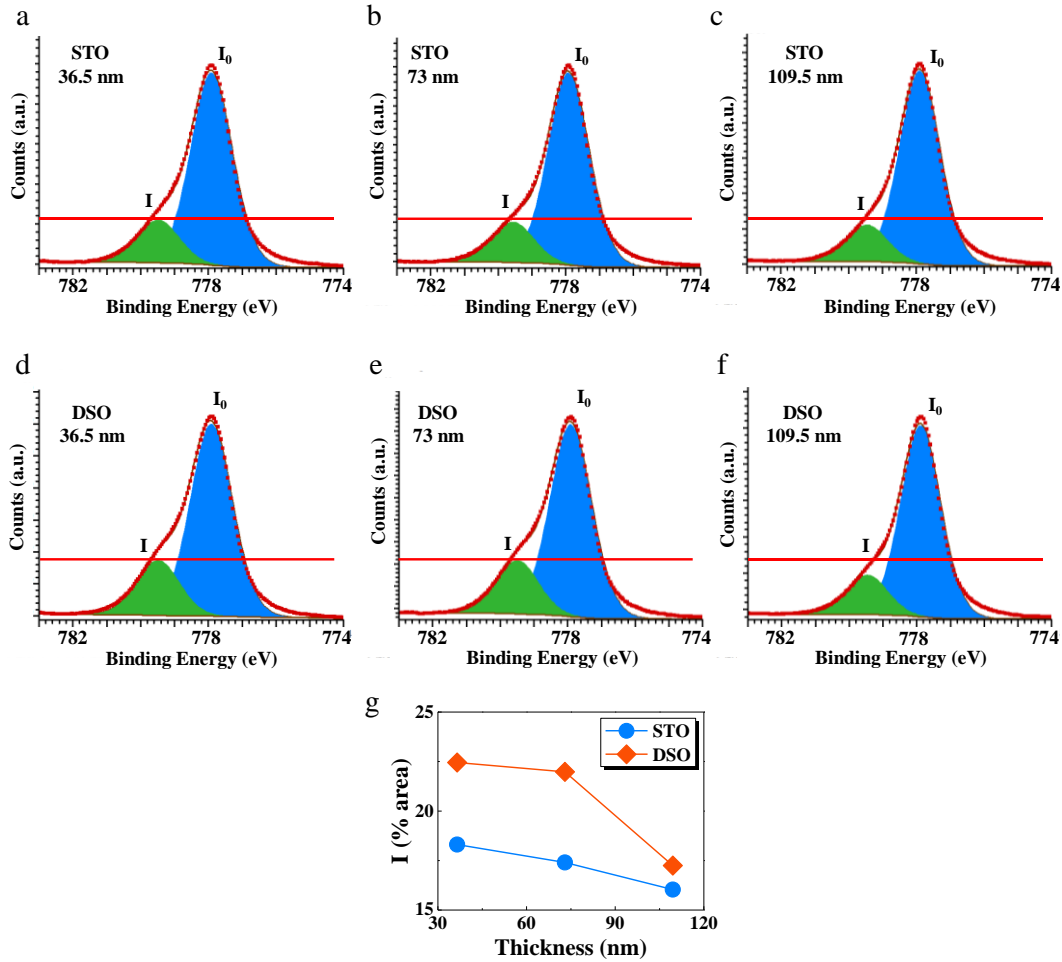


**Figure S15.** XPS normalized spectra of the six samples: XPS spectra of Ba 3d<sub>5/2</sub> core level. (a,b,c) 36.5, 73 and 109.5 nm thick BTO films grown on LSMO//STO substrate, respectively. (d,e,f) 36.5, 73 and 109.5 nm thick BTO grown on LSMO//DSO substrate, respectively. The fitting was performed as described in the Methods section by decomposing the area above the background into 2 contributions: the main BTO peak (labelled I<sub>0</sub>) and the BaCO<sub>3</sub> contribution<sup>14</sup> (labelled I) as indicated in panel (a). Red line indicates the maximum of the high energy contribution for the thinnest film of each set of samples to serve as eye-guide to compare its decreasing contribution for increasing thickness (g) Dependence of BaCO<sub>3</sub> intensity fraction on sample thickness.

**Table S1.** Data extracted from O 1s XPS spectra of BTO surface before and after steam treatment. The percentage of each contribution is defined as:  $A(j) (\%) = A(j) / A(\text{Tot})$  ( $j = \text{I}_0, \text{I}, \text{II}, \text{III}$ ) where  $A(j)$  is the area under the corresponding peak in the O 1s XPS spectra before and after the steam treatment (Fig. 1(d,e)). The rough errors from fitted areas are indicated.

	<b>O 1s</b>				$\Delta P_r$
	<b>I<sub>0</sub></b> (BTO)	<b>I</b> (BaCO <sub>3</sub> /O <sub>L</sub> -H)	<b>II</b> (OH <sup>-</sup> )	<b>III</b> (OH <sup>-</sup> /H <sub>2</sub> O)	
as-grown	56.2±0.1%	27.3±0.2%	14.5±0.1%	2.0±0.1%	0%
<i>steam treatment</i>	42.2±0.1%	27.4±0.4%	26.8±0.1%	3.6±0.1%	54.3±4.2%

**Table S2.** Relative fractions of the I<sub>0</sub>, I, II and III contributions to O 1s peaks and contributions of BaCO<sub>3</sub> phase to Ba 3d5/2 peaks of BTO/LSMO on STO and DSO shown in Supporting Information Figure S15. The percentage of each contribution is defined as: A(j) (%) = A(j) / A(Tot) (j = I<sub>0</sub>, I, II, III and BaCO<sub>3</sub> in Ba 3d5/2), where A(j) and A(Tot) indicate the area of j contribution and the total area of whole spectrum above the background. The errors from fitted areas are indicated

Substrate	t (nm)	O 1s				Ba 3d5/2	ΔP <sub>r</sub>
		I <sub>0</sub> (BTO)	I (BaCO <sub>3</sub> / O <sub>L</sub> -H)	II (OH <sup>-</sup> )	III (OH <sup>-</sup> /H <sub>2</sub> O)	BaCO <sub>3</sub>	
SrTiO <sub>3</sub>	36.5	60.6±0.2%	23.1±0.1%	14.6±0.1%	1.7±0.1%	18.3±0.1%	7.5±9.9%
	73	65.1±0.2%	20.1±0.2%	13.0±0.1%	1.8±0.1%	17.4±0.1%	6.5±6.0%
	109.5	61.4±0.1%	14.5±0.2%	16.8±0.2%	7.3±0.1%	16.0±0.1%	56.4±1.3%
DyScO <sub>3</sub>	36.5	60.6±0.4%	18.6±0.2%	18.7±0.1%	2.1±0.2%	22.4±0.1%	52.5±3.2%
	73	56.7±0.1%	18.0±0.1%	22.7±0.2%	2.6±0.1%	22.0±0.1%	68.6±4.9
	109.5	60.9±0.3%	13.1±0.1%	15.0±0.2%	11.0±0.1%	17.2±0.1%	76.8±3.0

## Supporting Information references

1. Fina, I.; Fàbrega, L.; Langenberg, E.; Martí, X.; Sánchez, F.; Varela, M.; Fontcuberta, J., Nonferroelectric Contributions to the Hysteresis Cycles in Manganite Thin Films: A Comparative Study of Measurement Techniques. *J. Appl. Phys.* **2011**, *109*, 074105.
2. Liu, F.; Fina, I.; Bertacco, R.; Fontcuberta, J., Unravelling and Controlling Hidden Imprint Fields in Ferroelectric Capacitors. *Sci. Rep.* **2016**, *6*, 2835.
3. Wemple, S., Polarization Fluctuations and the Optical-Absorption Edge in  $\text{BaTiO}_3$ . *Phys. Rev. B* **1970**, *2*, 2679.
4. CasaXPS. [www.casaxps.com](http://www.casaxps.com). Accessed date: 28/10/2016.
5. Tagantsev, A.; Gerra, G., Interface-Induced Phenomena in Polarization Response of Ferroelectric Thin Films. *J. Appl. Phys.* **2006**, *100*, 051607.
6. O'Neill, D.; Bowman, R.; Gregg, J., Dielectric Enhancement and Maxwell–Wagner Effects in Ferroelectric Superlattice Structures. *Appl. Phys. Lett.* **2000**, *77*, 1520-1522.
7. Lunkenheimer, P.; Bobnar, V.; Pronin, A.; Ritus, A.; Volkov, A.; Loidl, A., Origin of Apparent Colossal Dielectric Constants. *Phys. Rev. B* **2002**, *66*, 052105.
8. Pintilie, L.; Vrejoiu, I.; Hesse, D.; LeRhun, G.; Alexe, M., Extrinsic Contributions to the Apparent Thickness Dependence of the Dielectric Constant in Epitaxial  $\text{Pb}(\text{Zr},\text{Ti})\text{O}_3$  Thin Films. *Phys. Rev. B* **2007**, *75*, 224113.
9. Langenberg, E.; Fina, I.; Ventura, J.; Noheda, B.; Varela, M.; Fontcuberta, J., Dielectric Properties of  $(\text{Bi}_{0.9}\text{La}_{0.1})_2\text{NiMnO}_6$  Thin Films: Determining the Intrinsic Electric and Magnetoelectric Response. *Phys. Rev. B* **2012**, *86*, 085108.
10. Schmidt, R.; Ventura, J.; Langenberg, E.; Nemes, N. M.; Munuera, C.; Varela, M.; Garcia-Hernandez, M.; Leon, C.; Santamaria, J., Magnetoimpedance Spectroscopy of Epitaxial Multiferroic Thin Films. *Phys. Rev. B* **2012**, *86*, 035113.
11. Gutierrez, D.; Foerster, M.; Fina, I.; Fontcuberta, J.; Fritsch, D.; Ederer, C., Dielectric Response of Epitaxially Strained  $\text{CoFe}_2\text{O}_4$  Spinel Thin Films. *Phys. Rev. B* **2012**, *86*.
12. Liu, F.; Fina, I.; Gutiérrez, D.; Radaelli, G.; Bertacco, R.; Fontcuberta, J., Selecting Steady and Transient Photocurrent Response in  $\text{BaTiO}_3$  Films. *Adv. Electron. Mater.* **2015**, *1*, 1500171.
13. Malmberg, C.; Maryott, A., Dielectric Constant of Water from  $0^\circ$  to  $1000^\circ\text{C}$ .
14. Miot, C.; Husson, E.; Proust, C.; Erre, R.; Coutures, J., Residual Carbon Evolution in  $\text{BaTiO}_3$  Ceramics Studied by Xps after Ion Etching. *J. Eur. Ceram. Soc.* **1998**, *18*, 339-343.